Cancer Chemother Pharmacol (2011) 67:543–555
DOI 10.1007/s00280-010-1354-5

ORIGINAL ARTICLE

Reductive metabolism of the dinitrobenzamide mustard anticancer prodrug PR-104 in mice

Yongchuan Gu · Christopher P. Guise · Kashyap Patel · Maria R. Abbattista · Jie Lie · Xueying Sun · Graham J. Atwell · Maruta Boyd · Adam V. Patterson · William R. Wilson

Received: 15 March 2010 / Accepted: 28 April 2010 / Published online: 15 May 2010

Abstract
Purpose PR-104, a bioreductive prodrug in clinical trial, is a phosphate ester which is rapidly metabolized to the corresponding alcohol PR-104A. This dinitrobenzamide mustard is activated by reduction to hydroxylamine (PR-104H) and amine (PR-104M) metabolites selectively in hypoxic cells, and also independently of hypoxia by aldo-keto reductase (AKR) 1C3 in some tumors. Here, we evaluate reductive metabolism of PR-104A in mice and its significance for host toxicity.
Methods The pharmacokinetics of PR-104, PR-104A and its reduced metabolites were investigated in plasma and tissues of mice (with and without SiHa or H460 tumor xenografts) and effects of potential oxidoreductase inhibitors were evaluated.
Results Pharmacokinetic studies identified extensive non-tumor reduction of PR-104A to the 5-amine PR-104H (identity of which was confirmed by chemical synthesis), especially in liver. However, high concentrations of PR-104H in tumors that suggested intra-tumor activation is also significant. The tissue distribution of PR-104M/H was broadly consistent with the target organ toxicities of PR-104 (bone marrow, intestines and liver). Surprisingly, hepatic nitroreduction was not enhanced when the liver was made more hypoxic by hepatic artery ligation or breathing of 10% oxygen. A screen of non-steroidal anti-inflammatory drugs identified naproxen as an effective AKR1C3 inhibitor in human tumor cell cultures and xenografts, suggesting its potential use to ameliorate PR-104 toxicity in patients. However, neither naproxen nor the pan-CYP inhibitor 1-aminobenzotriazole inhibited normal tissue reduction of PR-104A in mice.
Conclusions PR-104 is extensively reduced in mouse tissues, apparently via oxygen-independent two-electron reduction, with a tissue distribution that broadly reflects toxicity.

Keywords PR-104 · Nitroreduction · Bioreductive prodrug · Dinitrobenzamide mustard · Naproxen · Aldo-keto reductase 1C3

Introduction

Bioreductive prodrugs are designed to be activated by enzymatic reduction in tumors and are of ongoing interest as potential anticancer agents [1–5]. Their selective activation within tumors can be achieved through hypoxia-dependent one-electron reduction, via a radical intermediate that is reoxidized by dioxygen [2, 6, 7]. Hypoxia represents a therapeutic target in tumors because it is more extreme than in normal tissues [8, 9], is responsible for resistance to cytotoxic agents through multiple mechanisms [3], and also contributes to failure of localized treatment (surgery and radiotherapy) by enhancing tumor

Electronic supplementary material The online version of this article (doi:10.1007/s00280-010-1354-5) contains supplementary material, which is available to authorized users.

Y. Gu · C. P. Guise · K. Patel · M. R. Abbattista · J. Lie · G. J. Atwell · M. Boyd · A. V. Patterson · W. R. Wilson (✉)
Auckland Cancer Society Research Centre,
Faculty of Medical and Health Sciences,
The University of Auckland, Private Bag 92019,
Auckland, New Zealand
e-mail: wr.wilson@auckland.ac.nz

X. Sun
Department of Molecular Medicine and Pathology,
Faculty of Medical and Health Sciences,
The University of Auckland, Auckland, New Zealand

invasion and metastasis [10]. Alternatively, some bioreductive prodrugs are substrates for oxygen-independent two-electron reduction (via NAD(P)H-dependent hydride transfer reactions), which can also offer selectivity for specific tumors in which the required oxidoreductases are highly expressed [11, 12].

Many bioreductive prodrugs depend on reduction of a nitro group for activation (e.g., CB1954, PR-104 and TH-302, which are currently in clinical development). However, an important limitation in the development of nitro compounds for this and other applications is that the enzymology of nitroreduction is poorly characterized. Although a number of mammalian enzymes have nitroreductase activity [2, 13], the rarity of nitro compounds as natural products suggests that their metabolic reduction is probably an incidental feature of enzymes that evolved to reduce other redox centers in cellular metabolites. Similarly, there have been relatively few quantitative studies of nitroreduction in mammals, and ongoing uncertainty as to which enzymes and tissues are most important.

Here we examine the reduction, in mice, of the 3, 5-dinitrobenzamide-2-nitrogen mustard PR-104 (Fig. 1a) which is in clinical trial as a bioreductive prodrug [14, 15]. This phosphate ester is hydrolyzed rapidly in vivo to the corresponding alcohol PR-104A [16], which is then metabolized selectively under hypoxia to the corresponding 5-hydroxylamine PR-104H and to an amine PR-104M [14, 17]; the latter is assumed to arise from further reduction of PR-104H (Fig. 1a). Reduction of the nitro group in dinitrobenzamide mustards to a hydroxylamine or amine acts as an electronic switch to increase the alkylating reactivity of the latent nitrogen mustard moiety [18], resulting in hypoxia-selective cytotoxicity in cell culture via DNA crosslinking [14, 17, 19]. Thus, nitroreduction is central to the intended mechanism of action and tumor selectivity of PR-104, but whether it also contributes to its normal tissue toxicity is not clear.

Two human enzymes catalyzing reductive activation of PR-104A have been identified in tumor cell lines. The first is the one-electron reductase NADPH:cytochrome P450 oxidoreductase (CYPOR, EC 1.6.2.4), identified as a PR-104A reductase under hypoxia by overexpression and RNAi studies [19, 20] which also demonstrate that this enzyme accounts for approximately 2/3 of the hypoxia-dependent

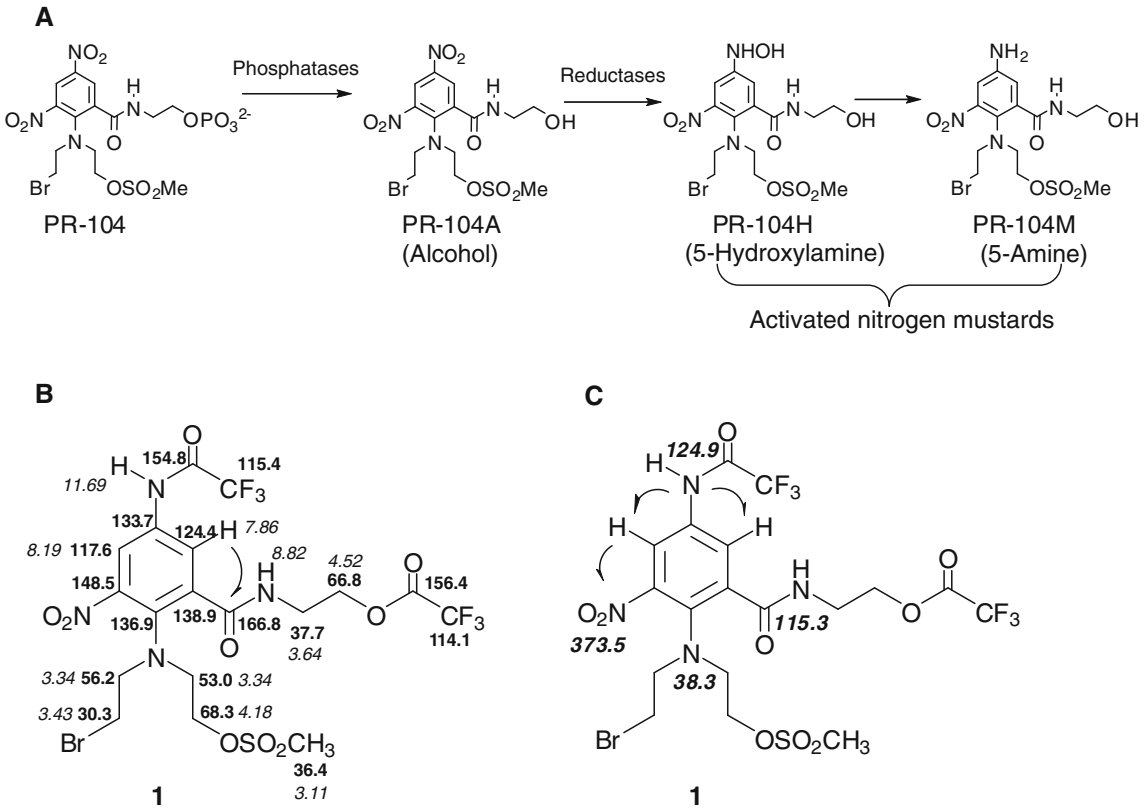

Fig. 1 **a** Structures of compounds investigated. PR-104 is hydrolyzed systemically to alcohol PR-104A, which is activated by reduction to the DNA crosslinking agents PR-104H and PR-104M in tumors and normal tissues. (**b**, **c**) Structural determination of **1** by one- and two-dimensional NMR experiments, identifying it as the ditrifluoracetyl derivate of PR-104M. **b** Chemical shifts for ^{1}H (*italics*) and ^{13}C (*bold*) resonances. The *arrow* shows the 3-bond ^{1}H–^{13}C HMBC cross peak. **c** Chemical shifts for ^{15}N (*bold italics*). *Arrows* show 3-bond ^{1}H-^{15}N HMBC cross peaks

PR-104A reduction in SiHa cells [20]. The second PR-104A reductase to be identified is a two-electron reductase, aldo-keto reductase (AKR) IC3 (prostaglandin F synthase, 17β-hydroxysteroid dehydrogenase type V), which reduces PR-104A to PR-104H under aerobic conditions [21]. AKR1C3 appears to be the only significant aerobic PR-104A reductase in human tumor cell lines, with NQO-1 playing no role in activation of this prodrug [20, 21].

Although highly expressed in some human tumors [21–23], AKR1C3 is also expressed in a range of normal tissues [24, 25] possibly including myeloid progenitors [26] which raises the question as to whether AKR1C3 (and orthologs in other species) might contribute to normal tissue toxicity of PR-104. The dose limiting toxicity of PR-104 in humans is myelotoxicity [15] as also observed in mice [14], rats and dogs [27], although in the rodent studies mucosal toxicity was also evident in the small intestine and hepatotoxicity was seen at doses above the MTD [27]. Whether these normal tissue effects are a consequence of PR-10A reduction is unknown. The recent development of sensitive LC–MS/MS methods for PR-104 metabolites [28] has made it possible to assay PR-104H and PR-104M in plasma of mice and cancer patients [29]. Here we evaluate the pharmacokinetics and tissue distribution of these reduced metabolites in mice, and the possible significance of one-electron (hypoxic) and two-electron (aerobic) PR-104A reductases in the toxicology of PR-104.

Materials and methods

Chemicals and reagents

PR-104, PR-104A [30], PR-104H [14], PR-104S1 [19], the tetradeuterated stable isotope internal standards of PR-104 (PR-104-d4) and PR-104A (PR-104A-d4), and PR-104 tritiated in the ethylcarboxamide side chain ([^{3}H]PR-104; specific activity 28.5 GBq/mmol, chemical purity 99%, radiochemical purity 94.4%; [31] were synthesized as reported. Stable isotope standards of PR-104H (PR-104H-d4), and PR-104M (PR-104M-d4) were prepared using the same methods as the non-deuterated compounds. All compounds had a purity of at least 95% by HPLC, and PR-104H and M were stored in acetonitrile as stock solutions at −80°C. Ketoconazole, cimetidine, isoniazid, metyrapone, quinidine, furafylline, celecoxib, naproxen, diethyldithiocarbamate (DDC) and 1-aminobenzotriazole (ABT) were from Sigma–Aldrich (St. Louis, MO). Indomethacin, ibuprofen, mefenamic acid, diclofenac and flurbiprofen were synthesized in-house. Acetonitrile (HPLC grade) was obtained from Merck (Darmstadt, Germany). Tissue solubilizer (Soluene-350) and liquid scintillants (Emulsifier-Safe^{TM}, Hionic-Fluor) were purchased from PerkinElmer, (Torrance, CA, USA). Other chemicals were all of analytical grade or higher purity.

Synthesis of PR-104M

A solution of PR-104A (1.25 g, 2.50 mmol) in dry MeOH (25 ml) was treated at room temperature with 10% Pd/C (1.25 g) followed by ammonium formate (0.75 g, 11.9 mmol). After being purged with N_2, the mixture was stirred at room temperature for 30 min under N_2, then filtered and the solution was concentrated under reduced pressure below 25°C and loaded onto a silica gel column. Elution with 2% MeOH/EtOAc gave a fraction that was concentrated to a small volume and diluted with hexane to give crude PR-104M (0.66 g, 56%), 2-[4-Amino (2-bromoethyl)-2-[[(2-hydroxyethyl) amino]carbamoyl]-6-nitroanilino]ethyl methanesulfonate, as a highly unstable gum that was stored immediately as a solution in dry acetonitrile at −80°C. ^{1}H NMR [$(CD_3)_2SO$] δ 8.40 (t, $J = 5.6$ Hz, 1H), 6.87 (d, $J = 2.7$ Hz, 1H), 6.71 (d, $J = 2.7$ Hz, 1H), 5.8 (br s, 2H), 4.11 (t, $J = 6.2$ Hz, 2H), 3.50 (t, $J = 6.3$ Hz, 2H), 3.37–3.15, after D_2O exchange (m, 8H), 3.12 (s, 3H), OH signal not observed. LRMS calculated for $C_{14}H_{21}^{79}BrN_4O_7S$, ($MH^+$) m/z 469.0, found 469.0; calculated for $C_{14}H_{21}^{81}BrN_4O_7S$, ($MH^+$) m/z 471.0, found 471.0.

A sample of PR-104M was converted to its stable derivative **1** (Fig. 1b) which was subjected to ^{1}H, ^{13}C, and ^{15}N NMR two-dimensional experiments, allowing structural confirmation of PR-104M. A solution of crude PR-104M (200 mg, 0.43 mmol) in 10:1 CH_2Cl_2/EtOAc (5 ml) was treated with trifluoroacetic anhydride (0.37 ml, 2.6 mmol) and stirred at room temperature for 5 min. The mixture was loaded onto a column of silica gel and elution with CH_2Cl_2/EtOAc (4:1) gave a fraction that was concentrated to a small volume and diluted with hexane to give **1** (227 mg, 81%), 2-(2-((2-bromoethyl)(2-(methylsulfonyloxy)ethyl)amino)-3-nitro-5-(2,2,2-trifluoroacetamido)benzamido)ethyl 2,2,2-trifluoroacetate, as a gum: ^{1}H NMR [$(CD_3)_2SO$] δ 11.69 (s, 1H), 8.82 (t, $J = 5.6$ Hz, 1H), 8.19 (d, $J = 2.6$ Hz, 1H), 7.86 (d, $J = 2.6$ Hz, 1H), 4.52 (t, $J = 5.2$ Hz, 2H), 4.18 (t, $J = 5.8$ Hz, 2H), 3.64 (q, $J = 5.3$ Hz, 2H), 3.47–3.30 (m, 6H), 3.11 (s, 3H). ^{13}C NMR [$(CD_3)_2SO$] δ 166.8, 156.4, 154.8, 148.5, 138.9, 136.9, 133.7, 124.4, 117.6, 115.4, 114.1, 68.3, 66.8, 56.2, 53.0, 37.7, 36.4, 30.3 HRMS (FAB^+) calculated for $C_{18}H_{20}^{79}BrF_6N_4O_9S$ (MH^+) m/z 661.0039, found 661.0055; $C_{18}H_{20}^{81}BrF_6N_4O_9S$ (MH^+) m/z 663.0018, found 663.0010.

PR-104A metabolism in aerobic cell cultures

Cell culture methods and origins of the cell lines are reported elsewhere [21]. Reductive metabolism of

PR-104A was assessed using confluent monolayers of H460, A549 or AKR1C3-overexpressing HCT116^{AKR1C3} cells using a modification of a previous method [19]. Cells (5×10^5 cells per well in 24-well plate) were pre-incubated at 37°C with inhibitors as required for 2 h, followed by addition of PR-104A to 100 μM (with maintenance of the inhibitor concentrations). Plates were incubated aerobically for a further 1 h, samples extracted with methanol containing PR-104H-d_4 internal standard as previously [19], and stored at −80°C for analysis by LC–MS/MS.

Animals and human tumor xenografts

All animal studies were approved by the University of Auckland Animal Ethics Committee (approvals AEC R279 and CR590) and complied with standards equivalent to the UKCCCR guidelines for the welfare of animals in experimental neoplasia [32]. Specific pathogen-free homozygous nu/nu (CD1-Foxn1^{nu}) mice (Charles River Laboratories, Margate, Kent, UK) were bred in the University of Auckland. Animals were housed in Techniplast microisolator cages in groups of 4–6 in a temperature-controlled room (20 ± 2°C) with a 12-h light/dark cycle and were fed ad libitum a sterilized rodent diet (Harlan Teklad diet 2018s). Tumors were grown subcutaneously on the right flank by inoculation of ~10^7 SiHa or H460 cells in 100 μl αMEM and dosed when tumors reached approximately 10 mm mean diameter.

Formulation, dosing, and evaluation of antitumor activity

PR-104 free acid was dissolved in PBS + 1 equivalent $NaHCO_3$ and diluted in PBS. [^{3}H]PR-104 was formulated in the same way after diluting with unlabelled PR-104 to a specific activity of 2.85 GBq/mmol. Naproxen and ABT were dissolved in 0.9% NaCl solution. Dosing solutions were prepared freshly, held at room temperature in amber vials, and used within 3 h. Tumor cell killing was assessed by excising tumors 18–24 h after treatment and assay of clonogenic cell survival in vitro as previously [14]. Log cell kill was calculated as $\log_{10}C - \log_{10}T$ where C is the mean clonogens/g tumor for controls (vehicle only) and T is the mean clonogens/g tumor for PR-104-treated mice. Significance of treatment effects were evaluated using one-way ANOVA followed by Holm–Sidak's test.

Plasma and tissue pharmacokinetics

Mice were dosed intravenously with PR-104 (562 μmol/kg, 326 mg/kg). At various times after dosing, blood was collected into EDTA-coated tubes, and tissue samples were collected within 3 min of termination. Plasma was immediately prepared by centrifugation (2,500–3,000 × g for 3 min) of blood, and plasma and tissues were rapidly frozen in liquid nitrogen before storage at −80°C for subsequent bioanalysis. In experiments requiring multiple tissues, to minimize dissection times one set of animals was used to collect the liver, kidney, pancreas, spleen, small intestine and tumor, while separate animals were used to collect heart, lung, brain and skeletal muscle. Bone marrow was collected from a third set of animals by dissecting both femurs and tibias, then excising the ends to allow extrusion of the marrow using a syringe with 22-gauge needle. Mice treated with [^{3}H]PR-104 were assayed similarly 48 h after dosing, except that tissues were minced, weighed (100–150 mg) and digested in 1.5 ml of Soluene-350 at 37°C overnight. Liver, spleen and lung digests were decolourized with 0.2–0.4 ml 30% H_2O_2 then warmed to 37°C for 15 min to decompose peroxides. After standing at room temperature for 1 h, 10–15 ml of Hionic-Fluor scintillant was added. Plasma samples (100 μl) were mixed with 10 ml Emulsifier-Safe scintillant and shaken vigorously. Radioactivity was measured using a liquid scintillation analyzer (Tri-Carb® 1500, Packard). Pharmacokinetic parameters were computed using WinNonlin (version 5.0, Pharsight, Mountain View, CA) via non-compartmental analysis.

Bioanalysis of PR-104 and metabolites

Plasma and tissue samples [16] and cell cultures [19] were extracted with methanol as previously reported. Samples (25 μl) were analyzed with an Agilent 1200 HPLC coupled with a triple quadrupole mass spectrometer (Model 6410, Agilent Technologies) by minor modification of a reported method [19]. Separation was achieved using an acetonitrile/water gradient on an Alltima C8 column (150 × 2.1 mm, 5 μ; Alltech) with 6 min run time. The m/z transitions monitored were 499 > 403 (PR-104A), 505 > 409 (PR-104A-d4), 485 > 389 (PR-104H), 491 > 395 (PR-104H-d4), 469 > 373 (PR-104M), 475 > 379 (PR-104M-d4) and, in the experiment for Fig. 5d, 393 > 297 for PR-104S, respectively. An external standard calibration curve was used for quantitation of PR-104S1. Naproxen was determined using an Agilent 1100 HPLC system with an acetonitrile/formate buffer gradient as reported [16] and quantified by absorbance at 270 nm with a photodiode array detector. Samples from the liver hypoxia models were analyzed using an Agilent 1200 Rapid Resolution system with a Zorbax SB-C18 (50 × 4.6 mm, 1.8 μm) column at 30°C with absorbance detection at 254 nm (PR-104M) and 370 nm (PR-104A). The mobile phase consisted of an acetonitrile/formate buffer gradient at a flow rate of 2.0 ml/min and run time of 4 min. Samples for Fig. 2b, c and ESM Fig. S3A

were analyzed using a LC/MS method reported previously [16].

Hepatic artery ligation model

Liver hypoxia was induced using a hepatic artery ligation method that exploits the dual circulation of the liver [33]. Mice were randomly assigned to two groups: control and ligation. After anesthesia with i.p. ketamine/xylazine (maintained throughout the experiment), a midline laparotomy was performed and the hepatic artery and portal vein were exposed. In the ligation group, the hepatic artery was dissected and disconnected with a cauterizer (Jorgensen laboratories Inc, Loveland, CO) under microsurgical microscopy, and the abdominal cavity was temporarily closed. 20 min later, the abdomen was re-opened and PR-104 was slowly injected via the hepatic portal vein (326 mg/kg, 5.6 µl/g body weight). Haemostasis was performed by applying a gauze on the injection site with pressure for 3 min. The abdomen was again temporarily closed. 15 min after the intraportal injection, blood was collected by cardiac puncture and the liver was removed. In the sham-operated control group, the mice were treated identically except that no ligation was performed.

Liver hypoxia in the model was evaluated in a separate experiment by immunofluorescence detection using pimonidazole (Hypoxyprobe^{TM}-1 Plus Kit; Natural Pharmacia International, Inc, USA). Pimonidazole was intraportally injected (60 mg/kg body weight) 10 min after hepatic artery ligation (or at the same time after laparotomy for the non-ligated group) and a control ligated animal received intraportal saline in place of pimonidazole. The abdominal cavity was closed and the liver was removed 25 min later.

Modulation of hypoxia with respiratory gases

Mice (4/group) were dosed i.v. with a mixture of PR-104 (326 mg/kg) and pimonidazole (60 mg/kg) in PBS, then placed in pre-equilibrated individual Techniplast microisolator cages flushed with carbogen (98% O_2/2% CO_2) or air or 10% O_2/90% N_2. Cages were flushed continuously with gases at 5L/min. Mice were killed and liver samples removed 30 min after dosing.

Immunohistochemical detection of hypoxia

Liver biopsies were formalin-fixed, embedded in paraffin and sectioned at 5 µm. Pimonidazole adducts were detected after antigen retrieval by boiling for 25 min in citrate buffer. The slides were washed with Tris-buffered saline (TBS) and blocked for 1 h in 3% bovine serum albumin-

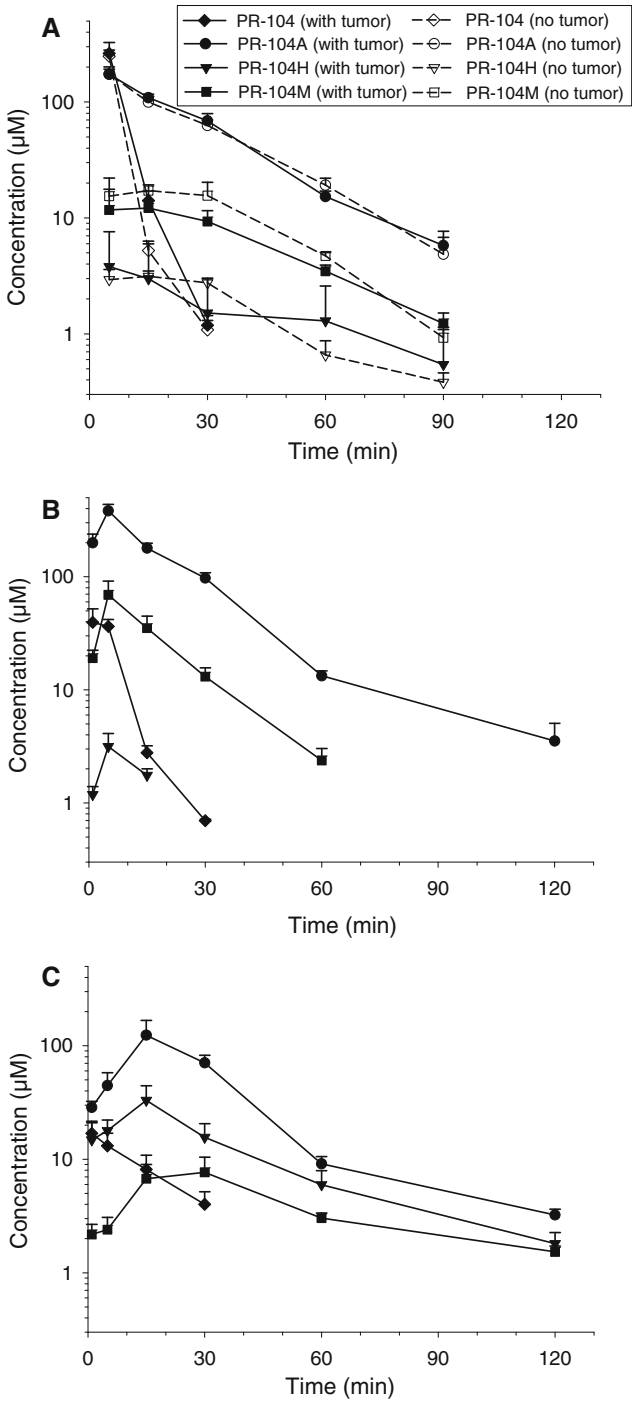

Fig. 2 Pharmacokinetics of PR-104, PR-104A and its reduced metabolites PR-104H and PR-104M in CD-1 nude mice following a single i.v. dose of PR-104 (326 mg/kg). *Points* are means and *bars* are SEM for 3 mice/group. *Open symbols* are for mice without tumors, and *filled symbols* for mice with s.c. SiHa tumors (8–12 mm diameter). The plasma values for mice with tumors are redrawn from Gu et al. [29]. **a** Plasma, **b** liver, **c** SiHa tumors

TBS followed by incubation at room temperature for 2 h with a 1:50 dilution of the fluorescein isothiocyanate-conjugated anti-pimonidazole monoclonal antibody (clone

4.3.11.3, Natural Pharmacia International, USA). Images were acquired at 4× magnification using a Nikon TE2000 inverted light/fluorescence microscope (Nikon Corp., Japan) under identical conditions for all samples within an experiment, and were analyzed using ImageJ to determine the proportion of pixels above a threshold set to best discriminate regions of positive staining.

Results

Synthesis and structural characterization of PR-104M

We recently reported [29] that a metabolite of PR-104 in mouse plasma has a low-resolution mass spectrum (MH^+ m/z 469, with a bromine 79/81 doublet) and absorbance spectrum consistent with its assignment as the 5-amine metabolite (PR-104M) which was earlier tentatively identified as a PR-104A metabolite in SiHa tumor cells [14]. Since this metabolite has not been rigorously characterized, we synthesized the 5-amine from PR-104A by regioselective reduction with Pd/C and ammonium formate in methanol. The resulting impure oil gave a ^{1}H NMR and low-resolution mass spectrum that confirmed reduction to an amine (see "Methods"). The unstable amine was converted to the stable *N*,*O*-ditrifluroacetyl derivative **1** which was subjected to ^{1}H, ^{13}C and ^{15}N NMR one- and two-dimensional experiments (Fig. 1b, c). Standard COSY, ^{1}H-^{13}C HSQC and ^{1}H-^{13}C HMBC were used to assign the resonances (δ values) in **1.** In particular, the 3-bond cross peak from the 7.86 ppm proton to 166.8 ppm carbon (Fig. 1b) confirmed the aromatic proton resonances. Cross peaks were seen from the NH at 11.69 ppm to both proton-bearing carbons (124.4 and 117.6 ppm), confirming the position of $NHCOCF_3$. This assignment was reinforced by the ^{1}H-^{15}N HMBC (Fig. 1c), which showed cross peaks from both aromatic protons to the nitrogen of $NHCOCF_3$ (124.9 ppm) but only from the 8.19 ppm aromatic proton to the nitro group nitrogen (373.5 ppm), thus confirming that PR-104M is the 5-amine rather than 3-amine.

Reduced metabolites of PR-104 in plasma, liver and tumor

Using synthetic PR-104M, PR-104H, PR-104A and PR-104 as standards for quantitation, and their tetradeuterated analogs as internal standards, we adapted a sensitive LC–MS/MS method [19] to assay all four species in mouse plasma and tissues. Representative chromatography is shown in ESM Fig. S1. Both PR-104H and PR-104M were readily detected in plasma 5 min after i.v. dosing of CD-1 nude mice with PR-104 (Fig. 2a). Non-compartmental pharmacokinetic parameters showed terminal half lives of PR-104H and PR-104M of ~20 min, similar to PR-104A itself (Table 1). The plasma AUC of PR-104M was ~20% of that for PR-104A, with lower concentrations of PR-104H. Concentrations of the reduced metabolites were the same in mice with and without SiHa tumors (Fig. 2a; Table 1) indicating that normal tissues provide the major source of reduced metabolites in plasma.

Consistent with this, concentrations of PR-104M were even higher in the liver than in the plasma of the same mice, again with PR-104M > PR-104H (Fig. 2b). We showed that the high levels in liver are not an artifact of postmortem hypoxic metabolism during sampling; when sampling of the liver was delayed for up to 10 min following termination, no significant changes in PR-104A and PR-104H were observed and PR-104M showed only a minor (<20%) increase (ESM Fig. S2). In contrast to liver, PR-104H rather than PR-104M was the major reduced metabolite in SiHa tumors (Fig. 2c), with an AUC 20-fold higher than in liver and sevenfold higher than in plasma (Table 1).

Tissue distribution of PR-104A and its reduced metabolites

The above pharmacokinetic studies indicated that reduced metabolites reach their maximum concentration in plasma within ~15 min (Fig. 2a). We used the same experimental

Table 1 Pharmacokinetics of PR-104A and its reduced metabolites in mouse plasma, liver and SiHa tumors in CD-1 nude mice after i.v. dosing with PR-104 at 326 mg/kg

	Tumor bearing	AUC (μmol h L^{-1})			$t_{1/2}$ (min)		
		PR-104A	PR-104H	PR-104M	PR-104A	PR-104H	PR-104M
Plasma	No	78.8[a]	2.7	14.3	16.3[a]	21.0	14.8
	Yes	81.6	3.0	10.2	16.8	23.9	20.5
Liver	Yes	140.6	1.1	22.3	19.0	11.8	11.4
Tumor	Yes	69.0	22.0	9.2	19.1	26.0	38.6

[a] Consistent with the previously reported AUC of 80 μmol h L^{-1} and $t_{1/2}$ of 13 min [14]

design to evaluate concentrations of PR-104A, PR-104H and PR-104M in a wider range of tissues in mice with SiHa tumors, 15 min after i.v. PR-104 (Fig. 3a). PR-104A concentrations were similar (100–400 μmol/kg) in most tissues, with SiHa tumors at the low end of this range. The exception was brain, with concentrations at least tenfold lower than any other tissue, suggesting lack of blood–brain barrier penetration. Reduced metabolites were detectable in all normal tissues, with PR-104M > PR-104H in all cases except in SiHa tumors where the hydroxylamine was the predominant metabolite, confirming the pattern seen in the time course studies. The total reduced metabolites (PR-104H plus PR-104M) varied widely between tissues, with highest levels in liver, followed by small intestine, then bone marrow, kidney and tumor. When normalized against PR-104A concentrations, levels of reduced metabolites were highest in tumor, followed by liver, kidney and bone marrow (Fig. 3b).

Residual radioactivity 48 h after dosing with [^{3}H]PR-104, presumably reflecting alkylation of macromolecules or formation of other long-lived cell-entrapped metabolites, represented approximately 2.3% of the injected dose (estimated by taking the median tissue, cardiac muscle, as representative). The residual radioactivity was also greatest in tumor and liver, which were the only tissues with levels significantly higher than plasma (Fig. 3c). We compared the total concentration of reduced metabolites (PR-104H and M) at 15 min and residual radioactivity at 48 h for the 11 tissues evaluated in both assays (averaging duodenum and jejunum/ileum to compare with total small intestine); this showed a highly significant correlation ($p = 0.01$, correlation coefficient 0.71) by Spearman correlation analysis.

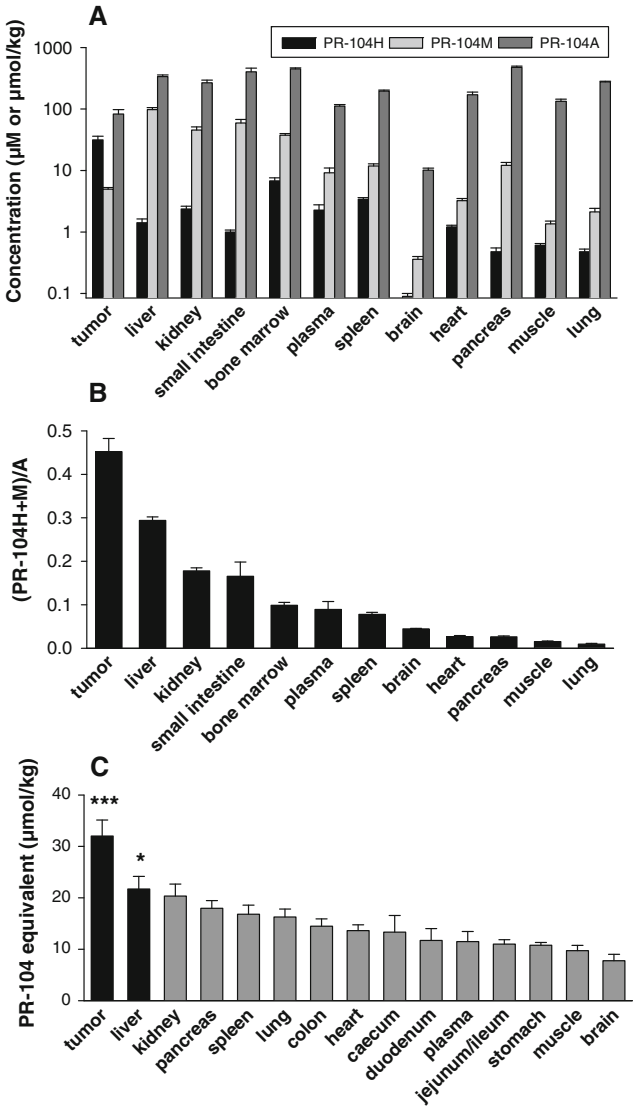

Fig. 3 Biodistribution of PR-104 metabolites in CD-1 nude mice with s.c. SiHa tumors following a single i.v. dose of PR-104 at 326 mg/kg. **a** PR-104A and its reduced metabolites PR-104H and PR-104M, determined by LC–MS/MS 15 min after dosing. Values are means and SEM for 5 mice. **b** Data from panel **a** redrawn to show total reduced metabolites normalized against PR-104A. **c** Residual radioactivity in tissues and plasma 48 h after dosing of [^{3}H]PR-104. Values are means and SEM for 3 mice. ***$p < 0.001$ and *$p < 0.05$ versus plasma by one-way ANOVA with Dunnett's test

Induction of hypoxia does not increase PR-104 reduction in mouse liver

The high levels of reduced PR-104A metabolites in liver raised the question as to whether this reduction depends on pericentral hypoxia in the liver [34], as would be expected if it is catalyzed predominantly by oxygen-sensitive one-electron reductases such as CYPOR. To examine this, we acutely increased liver hypoxia by hepatic artery ligation 20 min before administration of PR-104 via the hepatic portal vein. Induction of liver hypoxia was demonstrated, in separate mice, by dosing the hypoxia probe pimonidazole via the hepatic portal vein, which resulted in an obvious increase in its covalent binding in pericentral regions compared to non-ligated controls (Fig. 4a), as reported in other studies with the mouse hepatic artery ligation model [33]. In contrast, reductive metabolism of PR-104 to PR-104M was unchanged following hepatic artery ligation relative to sham-operated mice, as demonstrated by absolute concentrations of PR-104M and ratios of PR-104M/PR-104A as determined by HPLC (Fig. 4b). To confirm this apparent lack of oxygen sensitivity, we also compared mice that breathed 98, 21 or 10% O_2 for 30 min following i.v. dosing simultaneously with PR-104 and pimonidazole. Hypoxic gas breathing increased pimonidazole binding in the liver (Fig. 4c), although no effect of 98% O_2 on the weak binding in the air-breathing animals could be discerned. These conclusions were confirmed by image analysis (data not shown). Although systemic administration of PR-104 in this model provided higher PR-104A

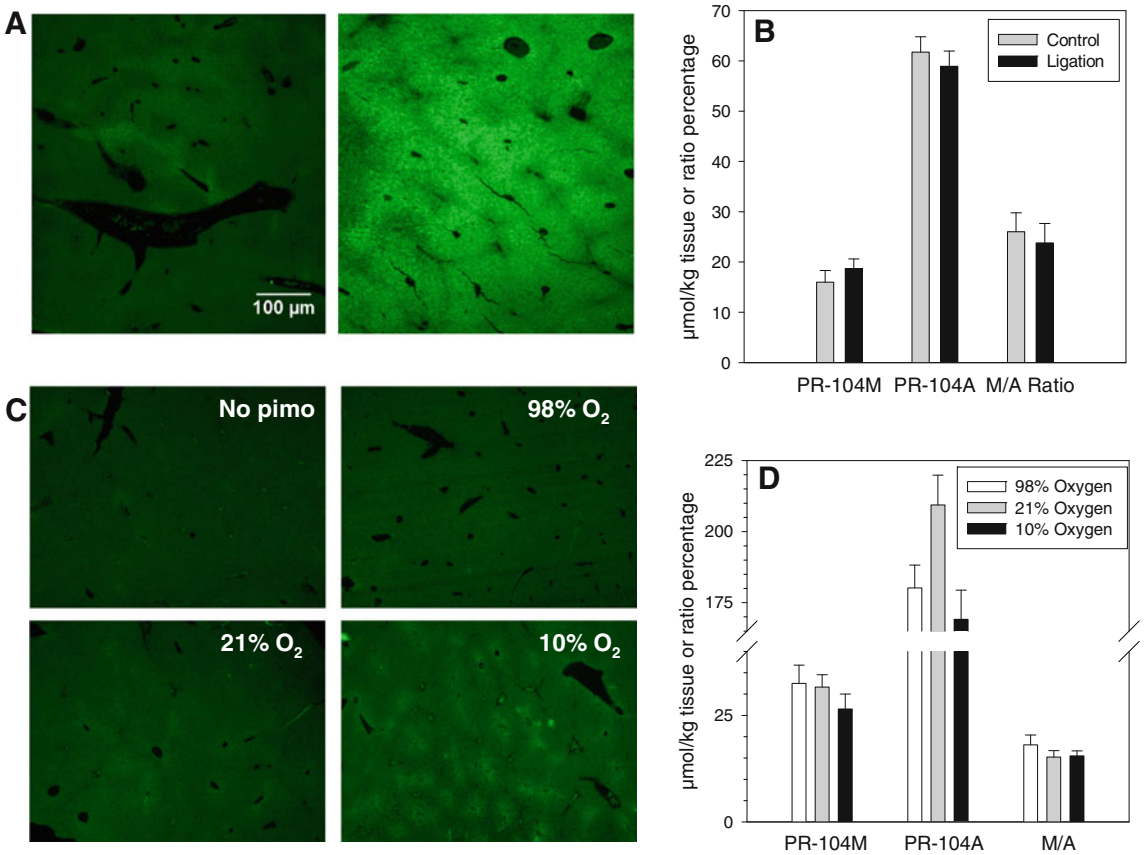

Fig. 4 Acute changes in liver hypoxia and effect on reductive metabolism of PR-104 following hepatic artery ligation (**a**, **b**) or modulation of respiratory gases (**c**, **d**). Images (**a**, **c**) show immunohistochemical detection of pimonidazole adducts for the mouse representing the median staining intensity of each group of 5-7 mice. **a** Pimonidazole was injected intraportally 10 min after hepatic artery ligation (*right*) or sham operation (*left*) and livers collected 25 min later for immunostaining. **b** Concentrations of PR-104A and PR-104M in liver, by HPLC, 15 min after intraportal administration of PR-104 (326 mg/kg) in mice with and without hepatic artery ligation. Values are mean and SEM for 5 (control) and 7 (ligation) mice. **c** Pimonidazole adducts in livers from mice held in 98% O_2/2% CO_2 (*top right*), air (*lower left*) or 10% O_2 (*lower right*) for 30 min after dosing with pimonidazole. The *top left* image shows autofluorescence in a sample from an air-breathing mouse that did not receive pimonidazole. **d** Concentrations of PR-104A and PR-104M in livers from the same groups as **c**

concentrations in liver than following intraportal administration, again there was no significant difference in PR-104M concentrations or PR-104M/PR-104A ratios between these three conditions (Fig. 4d). Thus, both models of acute liver hypoxia suggested that the predominant PR-104A oxidoreductase(s) in the mouse liver may be oxygen-insensitive.

Screening candidate inhibitors of PR-104A aerobic metabolism

Initial screening for inhibitors of aerobic PR-104A oxidoreductases was undertaken using aerobic cultures of A549 and H460 cells, which are fast metabolizers of PR-104A to PR-104H in the presence of oxygen [17]. This demonstrated significant inhibition by indomethacin, naproxen, mefenamic acid, ketoconazole and celecoxib but not by DDC or ABT (ESM Fig. S3A). It was subsequently shown that that the major aerobic PR-104A reductase in A459 and H460 cells is AKR1C3 [21]. We therefore further evaluated the effects of NSAIDs with known AKR1C3 inhibitory activity on PR-104A reduction in aerobic H460 cells (ESM Fig. S3B) and in an HCT116 cell line engineered to overexpress AKR1C3 (Fig. 5a). The IC_{50} values, summarized in Table S1, showed mefenamic acid, naproxen and indomethacin to be the most potent inhibitors in both cell lines, consistent with the reported sensitivity of AKR1C3 to these inhibitors in cell-free systems [35, 36]. Relative to achievable total plasma concentrations of these NSAIDs in humans, naproxen appeared to be the most promising AKR1C3 inhibitor (Table S1). The plasma pharmacokinetics of naproxen in mice appears not to have been reported, but in a pilot study we found that a single i.p. dose of 400 mg/kg provided plasma concentrations $\geq$2.5 mM between 15 and 120 min after dosing (ESM Fig. S4). Although protein binding is expected to be greater in

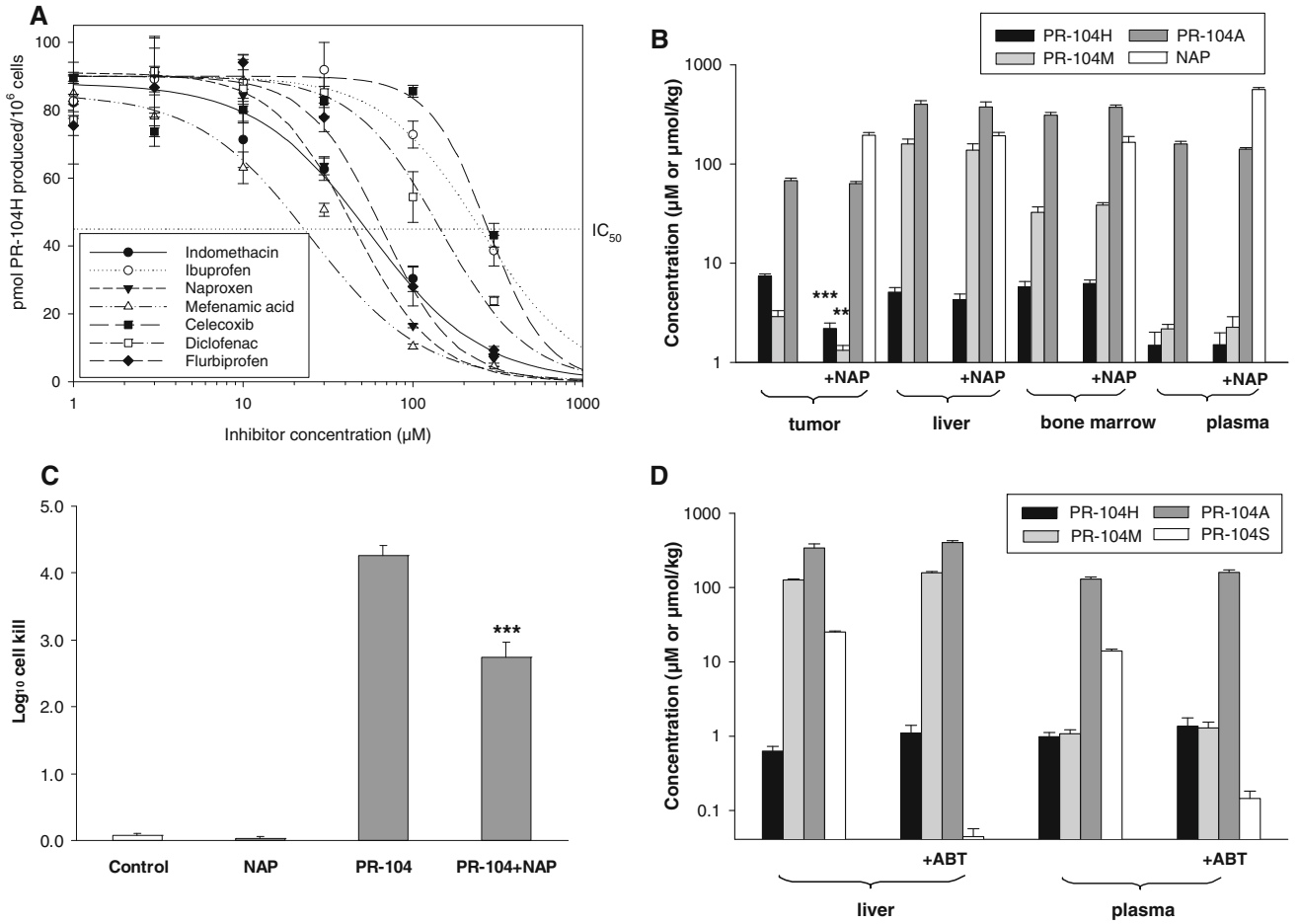

Fig. 5 Pharmacological inhibition of aerobic reduction of PR-104A in vitro and in mice. **a** Inhibition by NSAIDs of aerobic PR-104A reduction in HCT116^{AKR1C3} cell cultures. Inhibitors were added 2 h before PR-104A (100 μM), and PR-104H assayed by LC–MS/MS 1 h later. Values are means ± SEM for 3 determinations. The control value was 90.8 ± 5.2 pmol/10^6 cells. **b** Effect of pretreatment of mice with naproxen (NAP; 100 mg/kg i.p.) 30 min before PR-104 (326 mg/kg i.v.) on levels of PR-104A and its reduced metabolites in H460 tumors, plasma, liver and bone marrow assayed 15 min after PR-104. Values are means ± SEM for 5 mice. ***$p < 0.001$ and **$p < 0.01$ versus PR-104-only group by Student's t test. **c** Antitumor activity of PR-104 (326 mg/kg. i.v.) against H460 tumor xenografts in mice, by ex vivo assay of clonogenic cell survival 18 h after treatment, and effect of pretreatment with naproxen (100 mg/kg i.p.) 30 min before PR-104. Values are mean ± SEM for 6 mice. ***$p < 0.001$ versus PR-104 only group. **d** Effect of pretreatment of mice with 1-aminobenzotriazole (ABT; 100 mg/kg i.p.) 4 h before PR-104 (326 mg/kg i.v.) on levels of PR-104A, reduced metabolites and the oxidative dealkylation product PR-104S1, in plasma and liver assayed 15 min after PR-104. Values are means ± SEM for 5 mice

mouse plasma than in the cellular IC_{50} assays, this suggested use of naproxen to probe metabolism of PR-104A metabolism in mice.

Effects of naproxen and ABT on reductive activation of PR-104 in mice

Inhibition of PR-104 reductive metabolism in normal tissues and H460 tumors in mice was tested by dosing with naproxen (i.p., 100 mg/kg) 30 min prior to PR-104 (i.v., 326 mg/kg). Plasma and tissue samples were collected 15 min later, naproxen was assayed by HPLC, and PR-104A and its reduced metabolites by LC–MS/MS (Fig. 5b). Mean naproxen concentrations were 560 μM in plasma and 165–195 μM in tumor, liver and bone marrow. Naproxen had no effect on PR-104A levels, but significantly lowered concentrations of PR-104H and PR-104M in tumor with a 66% inhibition of total reduced metabolites. Consistent with this, in separate animals naproxen significantly ($p < 0.001$) inhibited the activity of PR-104 against H460 tumors as assessed using an ex vivo clonogenic cell survival assay (Fig. 5c). In contrast to the suppression of reductive activation in H460 tumors, naproxen had no effect on normal tissue levels of PR-104H or PR-104M (Fig. 5b). We also tested whether ABT, a pan-CYP inhibitor [37], inhibits reductive metabolism of PR-104A in mice. Administration of ABT (100 mg/kg, i.p.) 4 h before PR-104, conditions that have been demonstrated to provide effective CYP inhibition [38], had no effect on levels of PR-104H or PR-104M in liver or plasma (Fig. 5d). As a

positive control, we also monitored oxidative *N*-dealkylation of PR-104A to the semi-mustard metabolite PR-104S1 in this experiment; levels of PR-104S1 were reduced by >99.8% in liver and 99.0% in plasma, confirming CYP inhibition in this model. Thus reductive metabolism of PR-104A in mouse liver appears not to be due to CYPs.

Discussion

PR-104, a dinitrobenzamide mustard in clinical trial for targeting hypoxia [15], was designed to exploit the reduction of an electron-withdrawing nitro group to an electron-donating amine or hydroxylamine to activate a nitrogen mustard moiety [39]. When catalyzed by one-electron reductases, nitroreduction of the corresponding alcohol PR-104A is highly selective for hypoxic cells [14, 17, 19]. Recently activation by the two-electron reductase AKR1C3, which is overexpressed in some human tumors, has also been proposed as a mechanism of tumor selectivity of PR-104 [21]. The present study provides evidence for the selective reductive activation of PR-104A in tumor xenografts, and for a role of AKR1C3 in this process, but also demonstrates extensive reductive metabolism of PR-104A in normal tissues in mice.

A recent comparison of plasma metabolite profiles in mice and humans showed that PR-104M is the major reduced metabolite in mice, while PR-104H is dominant in humans [29]. The same species difference was seen in the present study, with PR-104M>H in all murine tissues (and plasma) but PR-104H>M in human (SiHa and H460) tumors (Figs. 3a, 5b). The identity of PR-104H as the 5-hydroxylamine (rather than the 3-hydroxylamine) has been established by ^{1}H-^{15}N gradient-enriched HMBC NMR [14]. Here we similarly prove that PR-104M is the 5-amine by NMR characterization of its stable trifluoroacetate derivative. Thus the 5-nitro group of PR-104A appears to be preferentially reduced by murine and human reductases.

The similar terminal half lives for elimination of PR-104A, PR-104H and PR-104M from mouse plasma (Table 1) suggests a quasi steady-state relationship between these species in which the reduced metabolites are cleared rapidly. Metabolite profiling in mouse plasma, bile and urine [29] indicates a wide range of other metabolites (predominantly thiol conjugates and *N*-dealkylation of the mustard) suggesting that nitroreduction is only one of several competing pathways of PR-104A metabolism. The availability of synthetic PR-104H and PR-104M will now make it possible to evaluate their pharmacokinetics following systemic administration and thus their rate of formation from PR-104A, their interconversion, and the extent to which this pathway contributes to overall PR-104A clearance.

The biodistribution study (Fig. 3) demonstrated relatively uniform tissue distribution of PR-104A 15 min after i.v. dosing (Fig. 3a), except for brain where levels were very low suggesting exclusion by the blood–brain barrier. PR-104H and PR-104M appear to be similarly excluded. Tumor concentrations of PR-104A were also modestly below plasma (Figs. 3a, 5b), presumably reflecting sparse vascularization. There were marked tissue differences in concentrations of reduced metabolites, although it is not clear whether these reflect differences in formation, subsequent metabolism or partitioning/uptake from plasma. Regardless, the PK profiles (Fig. 2) strongly suggest that liver is a major source of reduced metabolites in plasma. Thus concentrations of PR-104M reach a maximum at ~5 min in liver, well before than in plasma (Fig. 2a, b), and a constant ratio of PR-104M/PR-104A is established earlier in liver than plasma.

The concentrations of PR-104H and PR-104M in SiHa tumors also reach their maxima later than in liver (Fig. 2c), but this is also seen for PR-104A which likely reflects slow distribution of PR-104A into this poorly perfused compartment rather than redistribution from liver. The different metabolite ratios for SiHa tumors (PR-104H>M) than for the mouse normal tissues (PR-104M>H) also suggest that the PR-104H in these tumors is primarily generated within the tumors themselves, although oxidation of PR-104M to PR-104H in tumors remains a theoretical possibility. These observations suggest that PR-104A is acting at least in part as a locally activated prodrug within tumors, rather than only via hepatic activation which is considered the major route of activation of cyclophosphamide and related oxazaphosphorine nitrogen mustards [40]. Again, systemic administration of the active PR-104H and PR-104M metabolites would help clarify to what extent the circulating reduced metabolites might contribute to cytotoxicity and whether they might themselves be differentially metabolized in tumors and normal tissues.

Residual radioactivity in tissues 48 h after dosing with [^{3}H]PR-104 showed a significant correlation with concentrations of total reduced metabolites 15 min after dosing, suggesting that the residual radioactivity may be partially due to covalent binding of the activated alkylating metabolites. However, in cell culture studies covalent binding of [^{3}H]PR-104A by anoxic SiHa cells was inefficient (23 pmol/10^{6} cells per hour at 10 μM PR-104A; A. Theil and W.R. Wilson, unpublished data) despite extensive reduction to PR-104H and PR-104M (~140 pmol/10^{6} cells at steady state) under these conditions [17]. Together with the observation that there is much greater difference between tissues in PR-104H/M levels than in residual radioactivity, these observations suggest that much of the retained label is due to other metabolites.

Both the initial reduced metabolite levels and residual radioactivity suggest greater reductive metabolism of PR-104A in SiHa tumors than in mouse normal tissues (Fig. 3), although this was not the case for H460 tumors where concentrations of reduced metabolites are lower than in liver and bone marrow (Fig. 5b). Notably, there is a suggestive link between high levels of PR-104H/M and toxicity; preclinical studies in mice demonstrate bone marrow, gastrointestinal and possibly liver toxicity, which are all tissues with relatively high concentrations of reduced metabolites.

The tissues with highest steady-state PR-104H and M/PR-104A ratios (tumor, liver, kidney, small intestine, bone marrow; Fig. 2b) are likely to be those with the highest net PR-104A reductase activity, but the extent to which this reflects differences in expression/activity of reductases or hypoxia is not clear. A role for hypoxia is possible given that there is evidence for physiological hypoxia in all these tissues [34, 41, 42]. We therefore acutely modulated oxygen concentrations in liver, during PR-104 exposure, using two different models (hepatic artery ligation and intraportal administration, or modified respiratory gases with systemic administration). In both cases, induction of more severe hypoxia as demonstrated by pimonidazole binding had no effect on metabolism of PR-104A to PR-104M. This finding is in marked contrast to the strong enhancement by anoxia of NADPH-dependent PR-104A reduction in mouse liver S9 preparations [29] determined using mice of the same strain and colony as the current study. In the in vitro metabolism study, anoxia increased PR-104H formation by 22-fold and PR-104M formation by 340-fold relative to 21% O_2. It is known from whole cell metabolism studies with SiHa cells that extreme hypoxia is required for efficient activation of PR-104A, with 50% inhibition of cytotoxic potency at only 0.13 μM O_2 (0.1 mmHg) [43]. Thus the most likely reason for the lack of increased PR-104A reductive metabolism when liver hypoxia is enhanced is that the pO_2 values are not low enough to activate the one-electron reduction of PR-104A. As a corollary, we infer that the major PR-104A reductase(s) in mouse liver, under physiological oxygen, are oxygen-insensitive two-electron reductases. It remains to be determined whether hypoxia plays a part in reduction of PR-104A in any normal tissues (or human tumor xenografts) in mice.

The identity of the PR-104A reductase(s) in mice has proved to be elusive, as it has for other nitro compounds. CYP enzymes are unlikely to be involved given that marked inhibition of oxidative metabolism of PR-104A in liver by the pan-CYP inhibitor ABT had no effect on PR-104A reduction (Fig. 5d). Unlike H460 tumors, PR-104A reduction in murine normal tissues was insensitive to naproxen (Fig. 5b). This does not necessarily preclude a role for a murine AKR1C3 ortholog, but the marked differences in sequence and substrate specificities of murine versus human AKR1C family members [44] makes it difficult to identify a candidate murine ortholog. In particular, the murine AKR1C family members lack the characteristic prostaglandin F synthase activity of AKR1C3 [44]. We have recently expressed 4 murine AKR1C genes (AKR1C12, 14, 18, 20) at high levels in HCT116 cells, but none of the transfected lines demonstrated increased PR-104A reduction or cytotoxicity (S.D. Holford, C.P. Guise, A.V. Patterson and W.R. Wilson; unpublished data). The distinctly different substrate specificities and tissue distribution of murine and human AKRs [44] call into question the validity of the mouse as a model for the toxicology of PR-104 in humans.

The demonstration that naproxen is an effective inhibitor of PR-104A reduction by AKR1C3 in human tumor cells both in vitro (Fig. 5a; ESM Fig. S3B) and in xenograft models (Fig. 5b) was a useful outcome of the present study. The resulting decrease in tumor cell killing (Fig. 5c) provides further evidence for the importance of AKR1C3 in the monotherapy activity of PR-104 in xenografts [21]. It further suggests the potential use of naproxen to moderate the toxicity of PR-104 in humans if this proves to be due to AKR1C3, although this would only be appropriate in patients with low AKR1C3 expression in tumors and for which hypoxic activation of PR-104A is the intended therapeutic strategy.

Acknowledgments This work was supported by the Health Research Council of New Zealand [Grant 08/103] and a Technology In Industry Fellowship to Y. Gu from the Foundation for Research, Science and Technology, New Zealand.

Conflict of interest statement William R. Wilson is a founding scientist, stockholder and consultant to Proacta, Inc. Adam V. Patterson is a consultant to Proacta, Inc.

References

1. Workman P, Stratford IJ (1993) The experimental development of bioreductive drugs and their role in cancer therapy. Cancer Metastasis Rev 12:73–82
2. Wardman P (2001) Electron transfer and oxidative stress as key factors in the design of drugs selectively active in hypoxia. Curr Med Chem 8:739–761
3. Brown JM, Wilson WR (2004) Exploiting tumor hypoxia in cancer treatment. Nat Rev Cancer 4:437–447
4. McKeown SR, Cowen RL, Williams KJ (2007) Bioreductive drugs: from concept to clinic. Clin Oncol 19:427–442
5. Chen Y, Hu L (2009) Design of anticancer prodrugs for reductive activation. Med Res Rev 29:29–64
6. Mason RP, Holtzman JL (1975) The role of catalytic superoxide formation in the O_2 inhibition of nitroreductase. Biochem Biophys Res Commun 67:1267–1274
7. Siim BG, Wilson WR (1995) Efficient redox cycling of nitroquinoline bioreductive drugs due to aerobic nitroreduction in Chinese hamster cells. Biochem Pharmacol 50:75–82

8. Vaupel P, Schlenger K, Knoop C, Hockel M (1991) Oxygenation of human tumors: evaluation of tissue oxygen distribution in breast cancers by computerized O_2 tension measurements. Cancer Res 51:3316–3322
9. Tatum JL, Kelloff GJ, Gillies RJ, Arbeit JM, Brown JM, Chao KS, Chapman JD, Eckelman WC, Fyles AW, Giaccia AJ, Hill RP, Koch CJ, Krishna MC, Krohn KA, Lewis JS, Mason RP, Melillo G, Padhani AR, Powis G, Rajendran JG, Reba R, Robinson SP, Semenza GL, Swartz HM, Vaupel P, Yang D, Croft B, Hoffman J, Liu G, Stone H, Sullivan D (2006) Hypoxia: importance in tumor biology, noninvasive measurement by imaging, and value of its measurement in the management of cancer therapy. Int J Radiat Biol 82:699–757
10. Lunt SJ, Chaudary N, Hill RP (2009) The tumor microenvironment and metastatic disease. Clin Exp Metastasis 26:19–34
11. Skelly JV, Knox RJ, Jenkins TC (2001) Aerobic nitroreduction by flavoproteins: enzyme structure, mechanisms and role in cancer chemotherapy. Mini Rev Med Chem 1:293–306
12. Danson S, Ward TH, Butler J, Ranson M (2004) DT-diaphorase: a target for new anticancer drugs. Cancer Treat Rev 30:437–449
13. Walton MI, Wolf CR, Workman P (1989) Molecular enzymology of the reductive bioactivation of hypoxic cell cytotoxins. Int J Radiat Oncol Biol Phys 16:983–986
14. Patterson AV, Ferry DM, Edmunds SJ, Gu Y, Singleton RS, Patel K, Pullen SM, Syddall SP, Atwell GJ, Yang S, Denny WA, Wilson WR (2007) Mechanism of action and preclinical antitumor activity of the novel hypoxia-activated DNA crosslinking agent PR-104. Clin Cancer Res 13:3922–3932
15. Jameson MB, Rischin D, Pegram M, Gutheil J, Patterson AV, Denny WA, Wilson WR (2010) A phase I pharmacokinetic trial of PR-104, a nitrogen mustard prodrug activated by both hypoxia and aldo-keto reductase 1C3, in patients with solid tumors. Cancer Chemother Pharmacol 65:791–801
16. Patel K, Lewiston D, Gu Y, Hicks KO, Wilson WR (2007) Analysis of the hypoxia-activated dinitrobenzamide mustard phosphate prodrug PR-104 and its alcohol metabolite PR-104A in plasma and tissues by liquid chromatography-mass spectrometry. J Chromatogr B Analyt Technol Biomed Life Sci 856:302–311
17. Singleton RS, Guise CP, Ferry DM, Pullen SM, Dorie MJ, Brown JM, Patterson AV, Wilson WR (2009) DNA crosslinks in human tumor cells exposed to the prodrug PR-104A: relationships to hypoxia, bioreductive metabolism and cytotoxicity. Cancer Res 69:3884–3891
18. Helsby NA, Wheeler SJ, Pruijn FB, Palmer BD, Yang S, Denny WA, Wilson WR (2003) Effect of nitroreduction on the alkylating reactivity and cytotoxicity of the 2,4-dinitrobenzamide-5-aziridine CB 1954 and the corresponding nitrogen mustard SN 23862: distinct mechanisms of bioreductive activation. Chem Res Toxicol 16:469–478
19. Gu Y, Patterson AV, Atwell GJ, Chernikova SB, Brown JM, Thompson LH, Wilson WR (2009) Roles of DNA repair and reductase activity in the cytotoxicity of the hypoxia-activated dinitrobenzamide mustard PR-104A. Mol Cancer Ther 8:1714–1723
20. Guise CP, Wang A, Thiel A, Bridewell D, Wilson WR, Patterson AV (2007) Identification of human reductases that activate the dinitrobenzamide mustard prodrug PR-104A: a role for NADPH:cytochrome P450 oxidoreductase under hypoxia. Biochem Pharmacol 74:810–820
21. Guise CP, Abbattista M, Singleton RS, Holford SD, Connolly J, Dachs GU, Fox SB, Pollock R, Harvey J, Guilford P, Doñate F, Wilson WR, Patterson AV (2010) The bioreductive prodrug PR-104A is activated under aerobic conditions by human aldo-keto reductase 1C3. Cancer Res 70:1573–1584
22. Penning TM, Byrns MC (2009) Steroid hormone transforming aldo-keto reductases and cancer. Ann N Y Acad Sci 1155:33–42
23. Rizner TL, Smuc T, Rupreht R, Sinkovec J, Penning TM (2006) AKR1C1 and AKR1C3 may determine progesterone and estrogen ratios in endometrial cancer. Mol Cell Endocrinol 248:126–135
24. Penning TM, Burczynski ME, Jez JM, Hung CF, Lin HK, Ma H, Moore M, Palackal N, Ratnam K (2000) Human 3alpha-hydroxysteroid dehydrogenase isoforms (AKR1C1–AKR1C4) of the aldo-keto reductase superfamily: functional plasticity and tissue distribution reveals roles in the inactivation and formation of male and female sex hormones. Biochem J 351:67–77
25. Jin Y, Penning TM (2007) Aldo-keto reductases and bioactivation/detoxication. Annu Rev Pharmacol Toxicol 47:263–292
26. Birtwistle J, Hayden RE, Khanim FL, Green RM, Pearce C, Davies NJ, Wake N, Schrewe H, Ride JP, Chipman JK, Bunce CM (2009) The aldo-keto reductase AKR1C3 contributes to 7,12-dimethylbenz(a)anthracene-3,4-dihydrodiol mediated oxidative DNA damage in myeloid cells: implications for leukemogenesis. Mutat Res 662:67–74
27. Patel K, Holford N, Choy S, Hicks KO, Wilson WR (2010) A compartmental population pharmacokinetic model for the hypoxia-targeted dinitrobenzamide mustard prodrug PR-104 in humans, dogs, rats and mice. Cancer Chemother Pharmacol (submitted)
28. Gu Y, Wilson WR (2009) Rapid and sensitive ultra-high-pressure liquid chromatography–tandem mass spectrometry analysis of the novel anticancer agent PR-104 and its major metabolites in human plasma: application to a pharmacokinetic study. J Chromatogr B Anal Technol Biomed Life Sci 877:3181–3186
29. Gu Y, Atwell GJ, Wilson WR (2010) Metabolism and excretion of the novel bioreductive prodrug PR-104 in mice, rats, dogs and humans. Drug Metab Dispos 38:498–508
30. Denny WA, Atwell GJ, Yang S, Wilson WR, Patterson AV, Helsby NA (2005) Novel nitrophenyl mustard and nitrophenylaziridine alcohols and their corresponding phosphates and their use as targeted cytotoxic agents.PCT/NZ 2004/529249
31. Atwell GJ, Denny WA (2007) Synthesis of 3H- and 2H4-labelled versions of the hypoxia-activated pre-prodrug 2-[(2-bromoethyl)-2,4-dinitro-6-[[[2-(phosphonooxy)ethyl]amino]carbonyl]anilino]-ethyl methanesulfonate (PR-104). J Label Comp Radiopharm 50:7–12
32. (1988) UKCCCR guidelines for the welfare of animals in experimental neoplasia. Br J Cancer 58:109-113
33. Plock J, Frese S, Keogh A, Bisch-Knaden S, Ayuni E, Corazza N, Weikert C, Jakob S, Erni D, Dufour JF, Brunner T, Candinas D, Stroka D (2007) Activation of non-ischemic, hypoxia-inducible signalling pathways up-regulate cytoprotective genes in the murine liver. J Hepatol 47:538–545
34. Arteel GE, Thurman RG, Yates JM, Raleigh JA (1995) Evidence that hypoxia markers detect oxygen gradients in liver: pimonidazole and retrograde perfusion of rat liver. Br J Cancer 72: 889–895
35. Gobec S, Brozic P, Rizner TL (2005) Nonsteroidal anti-inflammatory drugs and their analogues as inhibitors of aldo-keto reductase AKR1C3: new lead compounds for the development of anticancer agents. Bioorg Med Chem Lett 15:5170–5175
36. Byrns MC, Steckelbroeck S, Penning TM (2008) An indomethacin analogue, *N*-(4-chlorobenzoyl)-melatonin, is a selective inhibitor of aldo-keto reductase 1C3 (type 2 3alpha-HSD, type 5 17beta-HSD, and prostaglandin F synthase), a potential target for the treatment of hormone dependent and hormone independent malignancies. Biochem Pharmacol 75:484–493
37. Ortiz de Montellano PR, Mathews JM (1981) Autocatalytic alkylation of the cytochrome P-450 prosthetic haem group by 1-aminobenzotriazole. Isolation of an NN-bridged benzyne-protoporphyrin IX adduct. Biochem J 195:761–764

38. Balani SK, Li P, Nguyen J, Cardoza K, Zeng H, Mu DX, Wu JT, Gan LS, Lee FW (2004) Effective dosing regimen of 1-aminobenzotriazole for inhibition of antipyrine clearance in guinea pigs and mice using serial sampling. Drug Metab Dispos 32:1092–1095
39. Denny WA, Wilson WR (1986) Considerations for the design of nitrophenyl mustards as agents with selective toxicity for hypoxic tumor cells. J Med Chem 29:879–887
40. Zhang J, Tian Q, Yung CS, Chuen LS, Zhou S, Duan W, Zhu YZ (2005) Metabolism and transport of oxazaphosphorines and the clinical implications. Drug Metab Rev 37:611–703
41. Vanderkooi JM, Erecinska M, Silver IA (1991) Oxygen in mammalian tissue: methods of measurement and affinities of various reactions. Am J Physiol 260:C1131–C1150
42. Parmar K, Mauch P, Vergilio J, Sackstein R, Down JD (2007) Distribution of hematopoietic stem cells in the bone marrow according to regional hypoxia. Proc Natl Acad Sci USA 104:5431–5436
43. Hicks KO, Myint H, Patterson AV, Pruijn FB, Siim BG, Patel K, Wilson WR (2007) Oxygen dependence and extravascular transport of hypoxia-activated prodrugs: comparison of the dinitrobenzamide mustard PR-104A and tirapazamine. Int J Radiat Oncol Biol Phys 69:560–571
44. Velica P, Davies NJ, Rocha PP, Schrewe H, Ride JP, Bunce CM (2009) Lack of functional and expression homology between human and mouse aldo-keto reductase 1C enzymes: implications for modelling human cancers. Mol Cancer 8:121–132